JOURNAL OF MATERIALS SCIENCE **34** (1999) 3355–3361

Microstructural features of an iron-based laser coating

XIAOLEI WU*, GUANGNAN CHEN
LNM Materials Research Center, Institute of Mechanics, The Chinese Academy of Sciences, 15 ZhongGuanCun Rd., Beijing 100080, People's Republic of China
E-mail: xlwu@cc5.imech.ac.cn

A high toughness wear resistant coating is produced by laser clad Fe-Cr-W-Ni-C alloys. The microstructural and compositional features of the laser-solidified microstructures and phase evolutions occurring during high temperature tempering at 963 K were investigated by using analytical electron microscopy with energy dispersive X-ray analysis. The clad coating possesses the hypereutectic microstructure consisted of $M_7C_3 + (\gamma + M_7C_3)$. During high temperature aging, the precipitation of $M_{23}C_6$ and M_2C in austenite and *in situ* transformation of dendritic M_7C_3 to $M_{23}C_6$ and eutectic M_7C_3 to M_6C occurred. The laser clad coating reveals an evident secondary hardening and superior impact wear resistance.

1. Introduction

The possibility of changing the surface composition and structure over a wide range as well as the creation of structures and non-equilibrium phases, render the laser cladding especially interesting and attractive [1–3]. By using laser-clad process, alloys containing large amounts of key alloying elements, such as high-speed steels and superalloys, can be fabricated.

There is considerable contemporary importance to develop cobalt free ferrous wear resistance material. Fe-Cr-C-X (X = Mn, W, Mo) alloys are excellent candidates [4, 5]. Singh and Mazumder [4] revealed wear properties of laser clad Fe-Cr-Mn-C alloys with metastable M_6C and M_7C_3 carbide precipitates to be superior to Stellite 6. Additionally, the high degree of grain refinement and increased homogeneity resulting from the rapid solidification can be expected to yield improved toughness. This is of great interest in the optimization of the microstructures. Komvopoulos and Nagarathnam [5] showed a uniform and hard cladding microstructures of Fe-Cr-W-C alloys with good resistance against shear deformation and microcracking. Recent studies on the wear of laser-treated high speed steel have shown that good toughness combined with high hardness is desirable to withstand the different wear mechanisms [6]. From the microstructural point, the existence of toughness austenite phase with a suitable volume fraction is considered to be helpful to the impact wear and fatigue wear, the main mechanism of which is considered to be the lack of ductility in the local region where the crack forms and grows [7]. With conventional heat treatment, it is difficult to increase toughness without a corresponding decrease in hardness. Thus, from the point of microstructure and alloying as well, to design a high toughness wear resistance clad coating is necessary.

Additionally, although microstructural modification of Fe-based alloys by laser clad with various compositions and process parameters has been demonstrated, a rather small amount of attention has been given to the microstructural characteristics and transformations of non-equilibrium and metastable phases especially at an elevated temperature, which control mechanical properties of the coating. Moreover, the emphasis is usually put on the wear behavior without a detailed linkage to the microstructural phenomena causing particular mechanical characteristics.

The objective of the present investigation, therefore, is to provide a comprehensive analysis of the crystal structures and microchemistries of phases in a homogeneous and hard clad coatings developed in the present study and to systematically track microstructure evolutions occurring during subsequent high temperature tempering at 963 K.

2. Experimental

The coating alloy is a powder mixture of Fe, Cr, W, Ni and C with a weight ratio of 10 : 5 : 1 : 1 : 1. Cr has a dual function, i.e., the predominant carbide former and an important alloying element in the matrix. W is the secondary hardening carbide former and provide additional strength to the matrix. Significant quantities of Ni are added to stabilize the fcc structure as a intrinsic toughness enhancer during service.

Laser-clad is carried out with a continuous wave 3 kW CO_2 laser equipped with a powder delivery system and an argon gas guidance device. A large amounts

* Author to whom all correspondence should be addressed.

of experiments are performed to quantify the effect of the laser clad parameters on the properties of the coating on a macroscopic scale, i.e., the thickness, the powder-clad efficiency, the volumetric dilution ratio and the crack formation in the coating [8]. Within the range of laser parameters the best results is at a 8 mm/s beam scanning speed, 3 mm beam diameter, 2 kW laser power, and 0.3 g/s feed rate, resulting in a mean coating thickness of 0.8 mm, a volumetric dilution ratio of about 7%, and free from the crack. The substrate material is 5CrMnMo in a quenched and tempered condition.

The as-solidified microstructures and phase transitions during high temperature aging at 973 K for 1 h are analyzed by JOEL-2000FX and Philips EM420 analytical transmission electron microscopy (ATEM). The chemical compositions of each phase are determined using energy-dispersive X-ray analysis (EDX) and EELS in conjunction with ATEM. The electron beam of ATEM EDX produce an electron spot of about 20 nm in diameter. Furthermore, the crystallographic phases of the coating are determined by standard X-ray diffraction techniques so as to support phase identification by TEM experiments.

Apart from above microstructural analyses, mechanical experiments are performed on the coating, including a Vickers hardness measurements and wear tests. The Vickers hardness measurements are carried out with a diamond indenter using a load of 0.2 kg. The impact wear is carried out by using MLD-10 Impact Wear Test Machine. Specimens for the test are ϕ 10 $\times$ 40 mm. Multiple laser tracks were used and the shift between two successive tracks was kept constant. The optimum shift used to ensure a constant thickness coating is determined to be about 25 pct of the beam diameter. Al_3O_2 particles of 380 mesh size was used as an abrasive. The impact work selected is 0.2 and 3 J respectively. The test parameters were at a flow rate of 180 g/min and impact frequency of 120 cycle/min. The friction counterpart was a hardened and tempered GCr15 steel (HRC62) rotated at a speed of 120 rpm.

3. Results and discussion

3.1. Laser-clad microstructures

Fig. 1 shows TEM micrographs of the laser-clad coating. The primary dendritic phase is determined to be M_7C_3 carbides (M = Cr, Fe, W, Ni), as shown in Fig. 1a. Fig. 1b reveals the interdendritic lamellar eutectic composed of (γ-austenite + M_7C_3). Thus, the microstructure is of hypereutectic feature, i.e., M_7C_3 + ($\gamma + M_7C_3$). Fig. 1c is SADP of the primary M_7C_3 and surrounded austenite in Fig. 1a, with a pseudohexagonal close-packed (hcp) crystal structure and the unit cell dimensions of crystal structure is $a_0 = 13.979$ Å and $c_0 = 4.618$ Å. Fig. 1d is SADP taken from an area covering an eutectic M_7C_3 and surrounding austenite of Fig. 1b.

The cooling rates are generally inversely proportional to the spacing of the dendrite arms. For the range of spacings between primary dendrites in the clad coating shown in Fig. 1a and from results for cooling rates of similar Fe-based alloys [9, 10], it may be postulated that the cooling rate is in a range of 10^3 to 10^5 K/s.

Additionally, a large amount of fine structures, such as high dislocation densities, stacking faults, and twins, exist in γ-austenite, as shown in Fig. 2.

The quantitative microchemistry of various phases is determined by EDX. The element contents of austenite

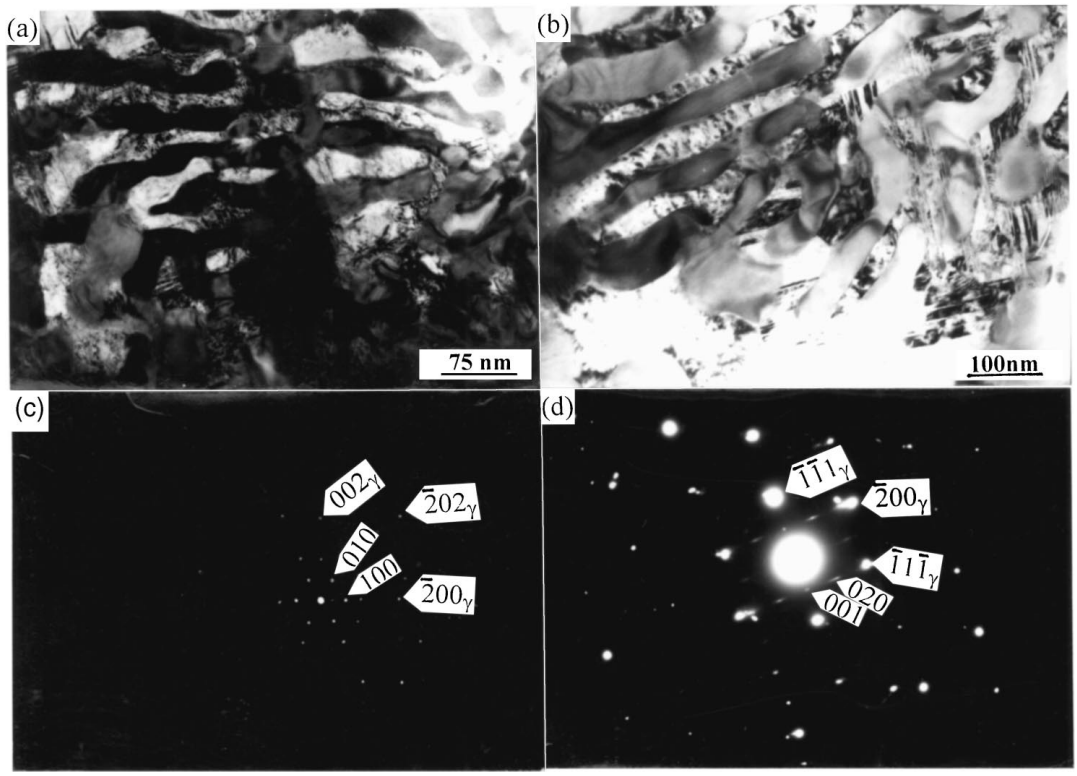

Figure 1 TEM micrographs showing the hypereutectic microstructure of the clad coating: (a) primary dendritic M_7C_3 carbide, (b) lamellar eutectic consisted of ($\gamma + M_7C_3$), (c) and (d) SADPs of M_7C_3 in (a) and of ($\gamma + M_7C_3$) in (b) respectively.

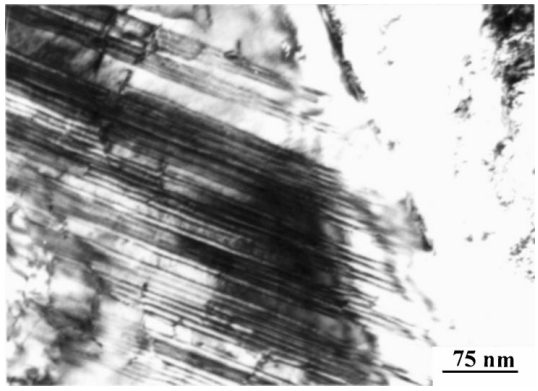

Figure 2 TEM micrographs showing a high density of dislocations and twins of eutectic austenite.

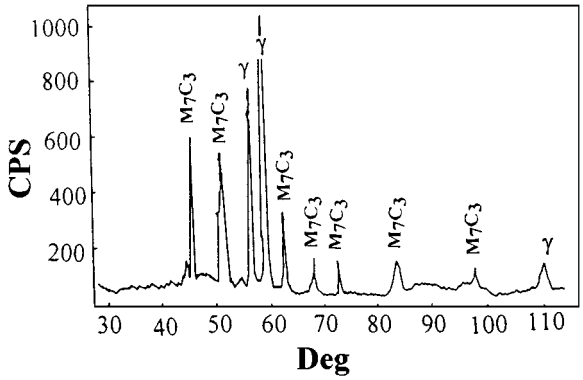

Figure 3 X-ray diffraction analysis of the as-cladded coating.

is 70.65Fe-16.68Cr-4.38W-4.45Ni-3.84C. The stoichiometries of both the dendritic and eutectic M_7C_3 are $Cr_{3.92}Fe_{2.75}W_{0.08}Ni_{0.25}C_3$ and $Cr_{4.02}Fe_{2.48}W_{0.32}Ni_{0.18}C_3$ respectively.

X-ray diffraction analysis, as shown in Fig. 3, indicates that the constituent phases of the laser-clad coating consist of γ-austenite and M_7C_3 carbides, well consistent with the above TEM observations. Typical volume fractions of the austenite and M_7C_3 carbides are approximately 42 and 58% respectively. It is noted that no bcc structure, such as δ-ferrite and martensite, is observed in the clad coating by TEM observation and X-ray analysis.

Based on the standard X-ray crystallographic procedures [11], the estimated lattice parameter of the γ fcc austenite is $a_0 = 3.674$ to 3.685 Å. Comparison of the experimentally determined d spacings with those given in the standard X-ray powder diffraction data, indicates that the lattice parameters of austenite in the produced coating are significantly greater than those obtained with conventional ingot metallurgical processing techniques. The enhancement of the lattice parameter of austenite suggests that significant dissolution of alloying elements, such as C, Cr, Ni, and W, commenced in the eutectic austenite. Therefore, the austenite is an nonequilibruim phase with extended alloy alloying contents and possess high density dislocations and stacking faults. The existence of eutectic austenite may be attributed to the lowing of the martensite-start temperature, the higher concentration of austenite stabilizing elements, and the high cooling rates. The retention of austenite in the present alloy system at room temperature is in agreement with the findings of other studies dealing with similar Fe-based alloys [4, 5].

Recent work by present authors [12] reveals that in the same alloy system, the primary solidification phase may be austenite only at a beam scanning rate high than 10 mm/s whereas the other laser processing parameters keeping constant. It is experimentally found that in the present investigation, an increase in the scanning rate causes a selection of the leading phase from M_7C_3 to austenite. The similar situation is also observed. It is noted that the change from δ to γ primary phase with the solidification rate, relevent to the beam scanning rate, is also observed in Fe-Cr-C austenitic stainless steels [13, 14]. This phenomena can be well explained by the kinetics of nucleation and growth of both phases [13]. Kurz [15] pointed out that in the case of directional solidification with a positive temperature gradient and if there is no barrier to nucleation, it is the leading solidification phase whose growth temperature is highest for a given speed. At the present investigation, the solidification process, in fact, is a non-equilibrium process, in spite of the relatively moderate solidification rates used.

The hardness of the austenite matrix and hard carbide phases determine the overall hardness of the clad coating. Despite a large proportion of austenite, the hardness of the as-cladded coating is remarkably high. The hardness is within the range 910 to 980 $Hv_{0.2}$. It increases with laser beam scanning speed, reflecting the influence of dendrite size and carbide volume fraction [8]. The higher hardness is stems from the formation of dendrite and eutectic Cr-rich M_7C_3 carbides. The hardness of M_7C_3 is about 1400 kgf/mm^2 [16] whereas the high hardness of austenite is explained by the small grain size, high solute content, and high dislocation density.

3.2. Carbide precipitation and evolution

The carbide type, size, and its distribution affect the mechanical properties of the laser-clad coating. The plate-shaped M_7C_3 carbide is considered to deteriorate hot workability and toughness. M_7C_3 is a meta-stable phase and its decomposition temperature is about 873 K [16]. Therefore, the dissolution and transformation of M_7C_3 may occur during high temperature aging. It is expected that more favorable carbide distribution can be obtained by the M_7C_3 decomposition. This occurs due to the fact that the M_7C_3 carbides can be easily decomposed in a short time at high temperatures. However, the decomposition behavior of M_7C_3 in the rapid solidification laser-clad layer has not been investigated in detail. The austenite is also an nonequilibruim phase and as a result, the precipitation reaction of various carbides is thermodynamically favorable.

Fig. 4a is a TEM micrograph revealing *in situ* transformation of dendritic M_7C_3 to $M_{23}C_6$ carbides. The dendritic M_7C_3 and fine granular $M_{23}C_6$ carbides are with a light and dark black contrast respectively. The $M_{23}C_6$ carbides are found to form on the interface of the M_7C_3 carbides and austenite matrix, as indicated by arrows. It is evident that nucleation of $M_{23}C_6$ occurs at the M_7C_3/austenite interfaces. In the case of tempering

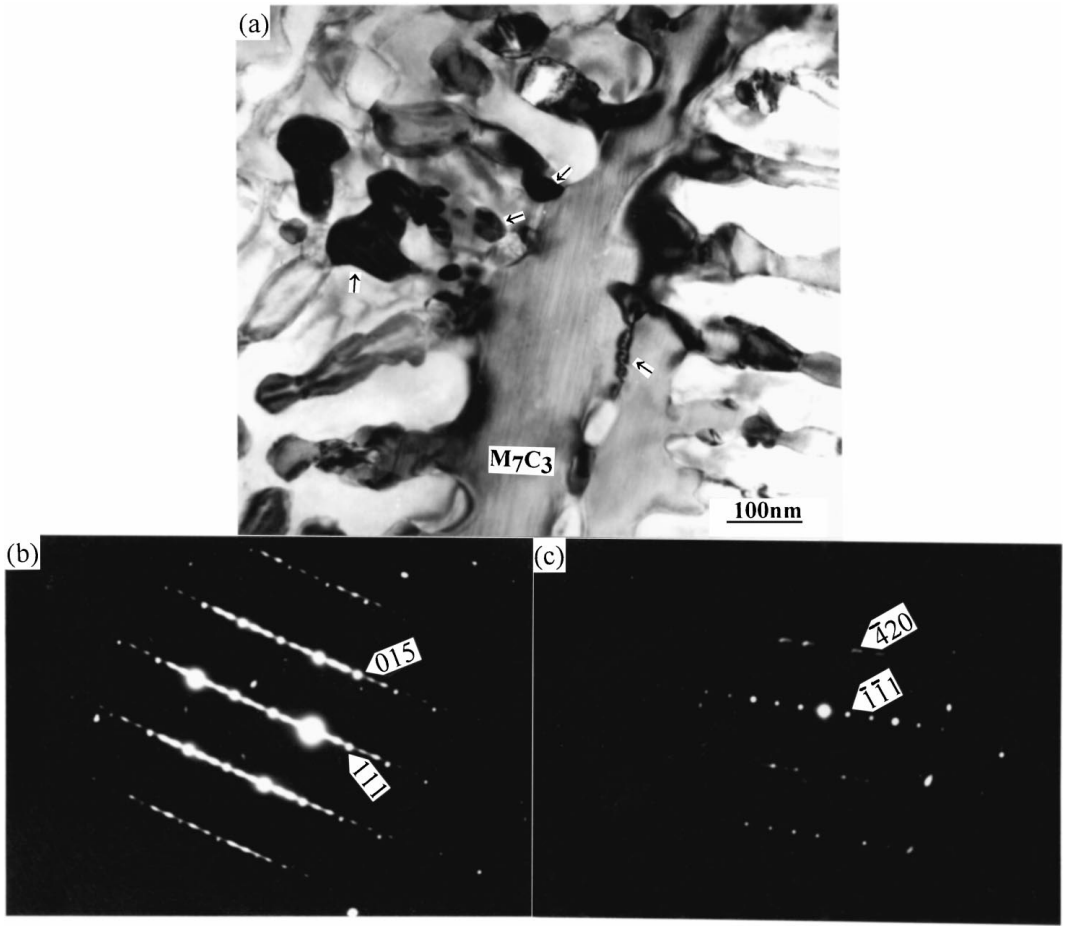

Figure 4 TEM micrograph showing *in situ* transformation of dendritic M_7C_3 to $M_{23}C_6$ carbides (a) SADPs of M_7C_3 (b) and $M_{23}C_6$ (c) respectively.

for a longer time or at a higher temperature, the $M_{23}C_6$ carbides grow from the outside inward and then the M_7C_3 carbides disappear. The decomposition behavior of dendritic M_7C_3 can be expressed as $M_7C_3 + \gamma \rightarrow M_{23}C_6$. Figs. 1b and c are SADPs of M_7C_3 and $M_{23}C_6$ carbides respectively. $M_{23}C_6$ is a Cr-Fe rich carbide and its stoichiometry is $Cr_{12.72}Fe_{10}W_{0.08}Ni_{0.2}C_6$ by EDX.

Fig. 5 is TEM micrographs revealing *in situ* transformation of eutectic M_7C_3 to M_6C carbides. The lamellar and large granular carbides both with a light black contrast are M_7C_3 in Fig. 5a and b, respectively. Fine granular carbides with a dark black contrast are determined to be M_6C-type carbides by SADP. Similar to the formation of $M_{23}C_6$, the M_6C carbides nucleate at the M_7C_3/austenite interfaces, as indicated by arrows, and proceed to grow. The formation of M_6C carbides may be described as $M_7C_3 + \gamma \rightarrow M_6C$. This transformation requires the partition of tungsten. In this case the supply of tungsten to form M_6C carbides can be provided by interface diffusion rather than volume diffusion in M_7C_3. This reaction, although starting at the interface, is sometimes also called *in situ* [17]. As this reaction proceeds, most of the eutectic M_7C_3 carbides is eventually replaced by M_6C carbides. According to the results of the EDX analysis of the tungsten content, the stoichiometry of M_6C carbides varies between $W_{3.8}Cr_{1.2}Fe_1C$ and $W_{3.4}Cr_{1.4}Fe_{1.2}C$.

The distinction between M_6C and $M_{23}C_6$ carbides is difficult because both structures are based on the same fcc bravais lattice with very close sizes of the unit cell, i.e., 1.113 nm and 1.086 nm, respectively. However, M_6C and $M_{23}C_6$ belong to Fd3m and Fm3m space groups respectively [18, 19]. M_6C and $M_{23}C_6$ are W-rich and Cr-Fe-rich carbides, respectively. Thus, it is easy to discriminate one from the other by using the extinction rules for the different space groups and by analysis of element compositions.

Carbide phase relations in the Fe-C-X (X = Cr, W, Mo, Ni etc.) systems have been great interest because of the importance of chromium, tungsten, and nickel as alloying elements in steels. Because of the different diffusion behavior of alloying elements at various temperatures, transient alloy carbide often form first which transform later into other alloy carbides. It is important to note that in alloyed steels these carbides can take place either by homogeneous nucleation within the pre-existing carbide (*in situ*) or by heterogeneous nucleation. The precipitation and *in situ* transition of alloy carbides have studied in conventionally treated steels [20, 21]. The *in situ* transformation sequency $M_3C \rightarrow M_7C_3 \rightarrow M_{23}C_6 \rightarrow M_6C$ was established in chromium alloyed steels [20]. The *in situ* transition has been observed for the reaction of M_7C_3 to $M_{23}C_6$ [21]. As for microstructures by laser *in situ* synthesis of ferrous coatings, however, there mainly exist non-equilibrium phases, the transition of which are not established especially during high temperature tempering.

Fig. 6a is a bright-field TEM micrograph illustrating plate-like $M_{23}C_6$ carbides with twin sub-structures precipitated around dislocations of the eutectic austenite. Fig. 6b is its SADP. $M_{23}C_6$ are determined to be

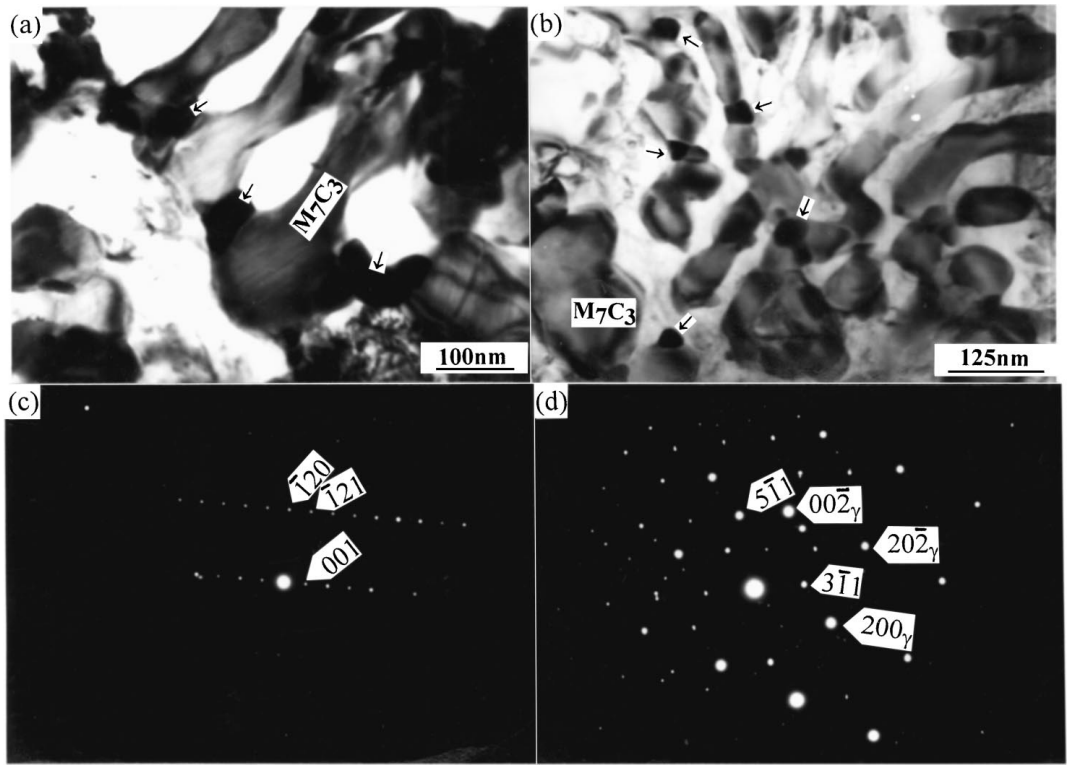

Figure 5 TEM micrographs showing *in situ* transformation of eutectic M_7C_3 to M_6C (a) and (b), (c) and (d) are SADPs of M_7C_3 and M_6C in (a) respectively.

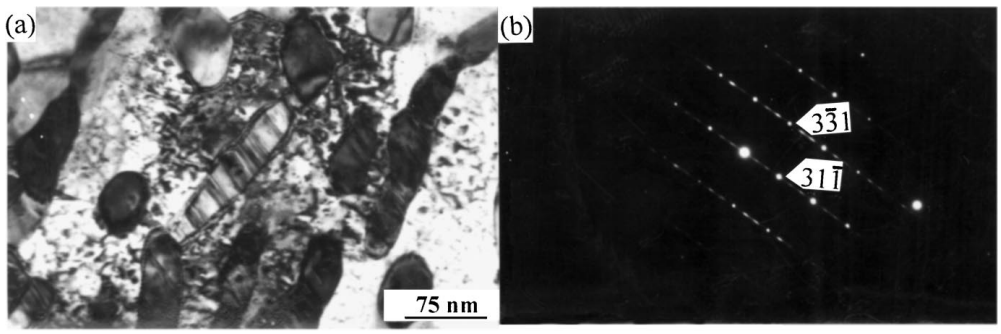

Figure 6 TEM micrograph showing plate-like $M_{23}C_6$ precipitated in austenite (a) and its SADP (b).

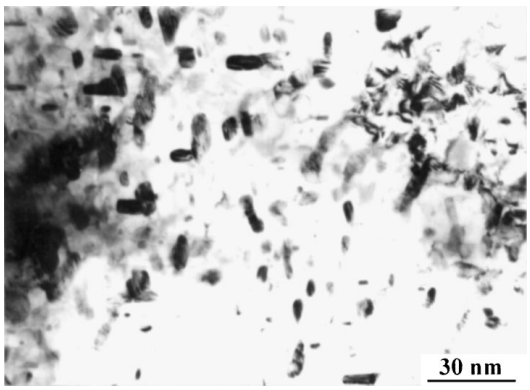

Figure 7 TEM micrograph showing M_2C carbides precipitated in austenite.

also Cr-Fe-rich carbides ($Cr_{11.75}Fe_{10.49}W_{0.02}Ni_{0.74}C_6$) by using EDX.

Fig. 7 reveals a bright-field TEM micrograph of small plate-like M_2C carbides mainly nucleated at dense dislocations in the eutectic austenite. They are W_2C carbides by diffraction analyses. In the peak-aged temperature of 690 °C, the fine M_2C carbides are densely dispersed and thus lead to a strong hardening. The size of carbides is in a range from 20 to 40 nm, and there is a evidence of carbides W_2C coarsening as a result of high temperature aging. The secondary hardening carbides often nucleate at the original carbide/matrix interface, dislocations, twin and lath boundaries and original austenite grain boundaries. The particles which nucleate at the original carbide/matrix interface and austenite GBs do not contribute significantly to strength, because nucleation sites are too scattered, but those which nucleate at dislocations and twin and lath boundaries make a large contribution to strength.

Since the precipitation of carbides is accompanied by a decrease in supersaturation, austenite will be destabilized and transform to martensite (α) during cooling, leading to a further increase in the overall hardness of the layey. The twin marensite formed in layer is illustrated in Fig. 8.

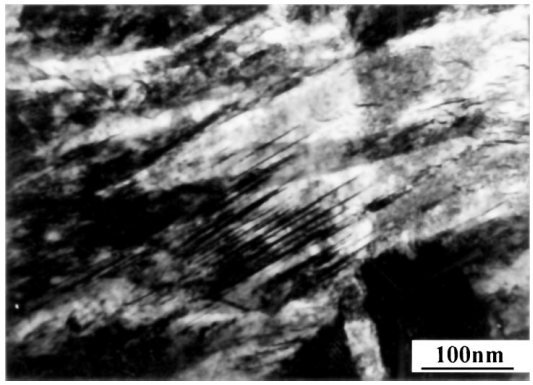

Figure 8 TEM micrograph showing the formation of aged martensite in clad microstructure during aging.

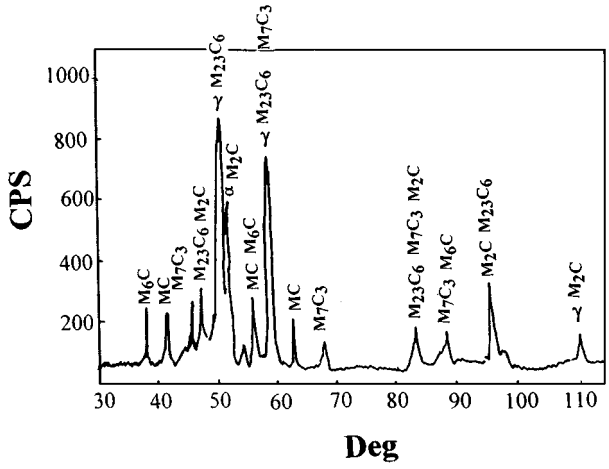

Figure 9 X-ray diffraction analysis of the peak-coating.

The above TEM observation is well consistent with phase analyses by X-ray diffraction, as shown in Fig. 9. Quantitative X-ray diffraction phase analysis reveals that the volume fraction of austenite is about 22 pct in peak-aged microstructures [8].

On the basis of the investigated results, the solidification and evolution sequence of phases can be represented as follows:

$$\begin{aligned} L \rightarrow M_7C_3 + L \rightarrow M_7C_3 + (\gamma + M_7C_3) \\ \rightarrow M_{23}C_6 + (\gamma + M_{23}C_6 + M_2C \\ + MC + \alpha + M_6C) \end{aligned}$$

3.3. Secondary hardening

Fig. 10 shows that the laser-clad coating possesses an evident secondary hardening feature. Secondary hardening behavior is due to the M_2C and MC carbide formation. The peak temperature and peak hardness are 690 °C and 1160 $Hv_{0.2}$ respectively. The higher secondary hardening temperature and peak hardness are mainly attributed to a delay in onset of disperse M_2C and MC precipitation. Another important fact that must be taken into account to explain the relative sluggishness of the precipitation reactions during tempering is that the diffusion coefficients of alloying elements in austenite are several orders of magnitude lower compared to ferrite or martensite [22]. As a result, secondary hardening will be delayed until higher temperatures.

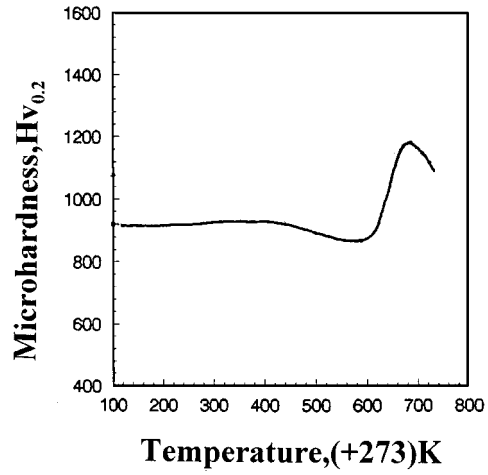

Figure 10 The secondary hardening curve of the clad coating.

The presence of large amounts of austenite has a strong influence on aging behavior. The austenite presents a higher solute content. As a result, austenite is very stable and only transform at temperatures where precipitation of alloy carbides occurs. In conventionally hardened steels, the most likely nucleation sites for carbides are the original austenite grain boundaries, and precipitation from austenite will not contribute significantly to hardness, but in the present coating austenite contains a high density of dislocations where carbides increase the hardness of the coating. The results show an intense precipitation of $M_{23}C_6$ and M_2C within austenite grains. Since these precipitation probably occurs by nucleation and growth on dislocations and other crystallographic defects, the precipitation are finely dispersed and, as a result, they will contribute significantly to strengthening the austenite and to retarding its recovery.

3.4. Wear resistance

Preliminary impact wear data for as-cladded and peak-aged microstructures are given in Fig. 11, as a function of impact work of 0.2 and 3 J, respectively. For all the data presented, each data point represents the average of at least three separate tests. For comparison, two additional values are also presented: data for conventional hardened and laser remelted AISI M4 high speed steel (HSS) respectively. The composition of HSS is 1.33C/4.3Cr/9.3W/4.9Mo/4.2V. The conventional hardened process is with quenching at 1250 °C and triple tempering at 560 °C for 2 h. After conventional hardening, samples are laser-remelted and parameters are 2 kW laser power, 3 mm beam diameter and 20 mm/s scanning speed. Laser-remelted samples are then post-heattreated at 600 °C for 2 h. The relative wear resistance is obtained by calculating the ratios of the measured weight change of conventionally treated HSS to that of laser-treated coatings.

It can be seen that the relative wear resistance of the peak-aged clad coating is highest. It is observed that the wear mechanism changes from microcutting to microcracking with impact work increasing from 0.2 to 3 J [8]. Basically, for laser-clad process to be effective against fatigue and impact wear, it should reduce surface and

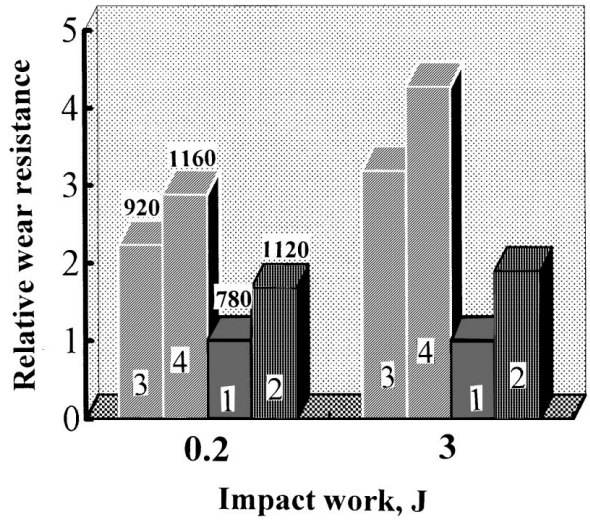

Figure 11 Relative wear resistance of clad coatings (hardness values indicated above bars); 1: Conventionally hardened HSS; 2: laser remelted HSS; 3: as-cladded microstructure; 4: peak-aged microstructure.

subsurface plastic deformation, microcrack initiation, and crack growth. The onset of microcracking depends on the fracture toughness of the materials and when microcracking become the predominant wear mechanism, the wear resistance will increase with an increasing fracture toughness [7]. An additional requirement is the good bonding of the coating to the substrate. Materials which have fine grained microstructures and exhibit high hardness and toughness are prime candidates for improve impact wear resistance. Komvopoulos and K. Nagarathnam [5] showed that the fine-grained austenite matrix with M_7C_3 carbide precipitates obtained by laser-cladded Fe-Cr-W-C alloy attributes to a higher resistance against plastic shear deformation and good toughness. Therefore, it can be concluded that the presence of a certain amount of ductile austenite in both as-cladded and peak-aged clad coating may be attributed to superior impact wear resistances.

The present laser clad microstructures can be considered as a composite material consisting of a ductile matrix and dispersely distributed carbides. Carbides contribute very substantially to the hardness of the clad layer. However, it is noted that there also remains a certain amount of austenite in as-aged and peak-aged microstructures respectively. The matrix is strengthened mainly by solid solution hardening due to W, Cr, and Ni, by Orowan looping around impenetrable carbides, and dislocation-dislocation interactions. By supporting the carbides the austenite prevents carbides from breaking loose during wear. Furthermore, the matrix also adjusts for both internal stress after laser cladding-to prevent cracking-and external stresses during wear. The austenite provides the coating ductility necessary to adjust for stresses imposed on the coating. As a result, the as-aged and peak-aged microstructures reveal superior impact wear resistances.

4. Summary

(1) The hypereutectic microstructure, i.e., $M_7C_3 + (\gamma + M_7C_3)$, is obtained by laser clad Fe-Cr-W-Ni-C alloys at present process conditions. The γ-austenite is non-equilibrium phase with extended solid solution and a great deal of crystal defects, i.e., high density dislocation, twins, and stacking faults.

(2) During high temperature tempering, there exist *in situ* carbide transformations, i.e., dendritic $M_7C_3 + \gamma \rightarrow M_{23}C_6$ and eutectic $M_7C_3 + \gamma \rightarrow M_6C$, and precipitation of $M_{23}C_6$ and M_2C carbides in austenite.

(3) The clad microstructure possesses evidently secondary hardening characteristics. The peak hardening temperature and peak hardness are 690 °C and 1250 $Hv_{0.2}$, respectively. The clad coating also reveals better impact wear resistance.

Acknowledgements

This research was supported by Major Science Research Foundation of The Chinese Academy of Sciences (KY951-A1-601-03), National Natural Science Foundation of China (59836220) and Postdoctor Research Foundation of China (4868).

References

1. C. W. DRAPER and J. M. POATE, *Int. Met. Rev.* **30** (1985) 85.
2. W. M. STEEN, *Metals and Materials* **1** (1985) 730.
3. J. MAZUMDER, "Surface Treatment and Film Deposition," edited by J. Mazumder, O. Conde, R. Villar and W. Steen, NATO ASI Series E: Applied Sciences-Vol. 307, 1996, p. 47.
4. J. SINGH and J. MAZUMDER, *Metall. Trans* **18A** (1987) 313.
5. K. KOMVOPOULOS and K. NAGARATHNAM, *J. Eng. Mater. Technol. Trans. of the ASME* **112** (1990) 131.
6. L. AHMAN, *Metall. Trans.* **15A** (1984) 1829.
7. K. H. ZUM GAHR, "Microstructure and Wear of Materials" (Elsevier, Amsterdam, 1987) p. 145.
8. X. L. WU, Postdoctor Thesis, Institute of Mechanics, The Chinese Academy of Sciences, Beijing 100080, 1998, p. 80.
9. K. NAGARATHNAM and K. KOMVOPOULOS, *Metall. Mater. Trans.* **26A** (1995) 2131.
10. J. F. FLINN, "Rapid Solidification Technology for Reduced Consumption of Strategic Materials" (Noyes Publications, Park Ridge, NJ, 1985) p. 42.
11. B. D. CULLITY, "Elements of X-Ray Diffraction" (Addison-Wesley, Reading, MA, 1978) p. 324.
12. X. L. WU and G. N. CHEN, *J. Mater. Sci. Lett* **17** (1998) 1849.
13. R. COLACO and R. VILAR, *Scripta Mater.* **36** (1997) 199.
14. W. LOSER and H. WERLACH, *Metall. Trans.* **23A** (1992) 1585.
15. W. KURZ, B. GIOVANOLA and R. TRIVEDI, *Acta Metall* **34** (1986) 823.
16. J. P. MORNIROLI, E. BAUER-GROSSE and M. GANTOIS, *Phil. Mag* **48A** (1983) 311.
17. A. T. DAVENPORT and R. W. K. HONEYCOMBE, *Met. Sci.* **9** (1975) 201.
18. P. B. HIRSCH *et al., Electron Microscopy of Thin Crystals* (Knieger, New York, 1977) p. 231.
19. T. F. LIU, S. W. PENG, Y. L. LIN and C. C. WU, *Metall. Trans. A* **21A** (1990) 567.
20. A. INOE and T. MASAMOTO, *ibid.* **11A** (1980) 739.
21. S. HAMAT-THIBAULT, M. DURAND-CHARRE and B. ANDRIES, *ibid.* **13A** (1982) 545.
22. R. VILAR, R. COLACO and A. ALMEIDA, "Surface Treatment and Film Deposition," edited by J. Mazumder, O. Conde, R. Villar and W. Steen, NATO ASI Series E: Applied Sciences, Vol. 307, 1996, p. 453.

Received 10 September 1998
and accepted 29 January 1999